Sensitivity of the Amery Ice Shelf, Antarctica, to Changes in the Climate of the Southern Ocean

M. J. M. WILLIAMS*

Danish Center for Earth System Science, Niels Bohr Institute for Physics, Geophysics and Astronomy, University of Copenhagen, Copenhagen, Denmark

R. C. WARNER

Antarctic CRC, and Australian Antarctic Division, Hobart, Australia

W. F. BUDD

Antarctic CRC, Hobart, Australia

(Manuscript received 26 February 2001, in final form 22 March 2002)

ABSTRACT

Coupled ocean–atmospheric general circulation models indicate that warming of up to 3°C may occur over the next century in waters immediately to the north of the Amery Ice Shelf. The impact of this warming on the ocean cavity under the Amery Ice Shelf and the mass exchange at the interface between the ocean cavity and the ice shelf is investigated using a three-dimensional ocean model. Warming of between 0.25° and 3.0°C is applied along the ice front in a series of model runs, rather than in a single transient run. Changes in salinity are also considered for larger amounts of warming. The model results show that the circulation in the ocean cavity changes as warming increases, particularly in the gyres that dominate the horizontal circulation. The changes in the heat flux from the warming increase the melt rates from the base of the Amery Ice Shelf, from the present-day mean melt rate and net mass loss estimates of 0.28 m yr^{-1} and 14.2 Gt yr^{-1}, respectively, by approximately 0.55 m $yr^{-1}°C^{-1}$ and 28.4 Gt $yr^{-1}°C^{-1}$. The maximum melt rates increase much more strongly, by around 10 m $yr^{-1}°C^{-1}$. These increased rates of melting suggest substantial modification of the ice shelf would occur in a warmer climate, particularly near the grounding line, and thus indicate that warming of the oceans around Antarctica has the potential for significant impact on the Antarctic ice sheet.

1. Introduction

Melting at the base of Antarctic ice shelves is a major source of ice loss from the Antarctic ice sheet (Jacobs et al. 1992). The rate at which it occurs is highly dependent on the temperature of the ocean waters adjacent to the ice shelves. Any change in ocean temperatures from variations in climate could thus impact on the ice shelves which fringe much of the Antarctic coast. While the impacts on the grounded ice sheet of a major modification to the state of the ice shelves are not fully resolved, modeling studies by Warner and Budd (1998) and Huybrechts and de Wolde (1999), indicate that increasing the basal melting beneath ice shelves could be influential in changing ice sheet volumes and global sea level on millennial timescales.

The Amery Ice Shelf is the third largest embayed ice shelf in Antarctica, and forms the floating portion of the Lambert Glacier system, a glacier system that drains a large fraction of the east Antarctic ice sheet. In this paper we investigate the sensitivity of the Amery Ice Shelf to changes in the climate of the Southern Ocean.

Ocean circulation under ice shelves is a unique problem, because the thickness of the ice shelf (from ~200 m at the ice front to well over 1000 m at the grounding line) provides a temperature gradient across the ocean cavity through the pressure dependence of the freezing temperature and insulates the ocean cavity from atmospheric forcing. Such a boundary condition effectively drives a heat pump that causes melting in the deeper regions of the cavity and some freezing in the shallower regions, with the exact details dependent on the induced circulation and the inflowing water temperatures.

A range of different models have been developed for the circulation in ocean cavities underneath ice shelves.

* Current affiliation: National Institute for Water and Atmospheric Research, Wellington, New Zealand.

Corresponding author address: Dr. Michael Williams, NIWA, P.O. Box 14 901, Kilbirnie, Wellington, New Zealand.
E-mail: m.williams@niwa.cri.nz

In a recent review, Williams et al. (1998a) identified the three most commonly used models as one-dimensional plume models (MacAyeal 1985; Jenkins 1991; Jenkins and Bombosch 1995), two-dimensional vertical overturning thermohaline models (Hellmer and Olbers 1989, 1991), and three-dimensional general circulation models (Determann and Gerdes 1994; Grosfeld et al. 1997).

The circulation regime beneath the Amery Ice Shelf has previously been investigated with two-dimensional (Hellmer and Jacobs 1992) and three-dimensional (Williams et al. 1998b; Williams 1999; Williams et al. 2001) modeling techniques. The most recent study (Williams et al. 2001) carried out an extensive investigation of the present-day circulation and thermohaline structure in the ocean cavity under the Amery Ice Shelf. In that study two different boundary conditions for the barotropic exchange at the ice front were investigated, and it was also found that the ocean circulation under the Amery Ice Shelf was largely barotropic and strongly influenced by the thickness of the water column.

Studies of the impact of changes in ocean temperature have been carried out on other ice shelves by Jenkins (1991), Hellmer and Jacobs (1995), and Grosfeld and Gerdes (1998). Jenkins (1991) used the plume model and found that the mean melt rate at the base of the Ronne Ice Shelf increased from 0.6 to 2.6 m yr^{-1}, when the -1.91°C layer of High Salinity Shelf Water (HSSW) under the Ronne Ice Shelf was rapidly replaced with a -1.3°C layer of Modified Warm Deep Water.

In their study of the Ross Ice Shelf in the vicinity of Roosevelt Island, Hellmer and Jacobs (1995) used their two-dimensional thermohaline model in a channel configuration. They gradually warmed the ocean forcing at each end of the cavity by 0.01°C yr^{-1} for 100 yr. After this time period they found the melt rate had increased from a mean of 0.18 to a mean of 1.38 m yr^{-1}. In a further experiment, Hellmer and Jacobs changed both the salinity and the temperature. The temperature change was the same as in the previous experiment, while the salinity forcing field was decreased from a mean of 34.5 psu, with an annual variation of 0.15 psu, by 0.02 psu yr^{-1} over the same timescale. This reduced the final mean melt rate to 0.98 m yr^{-1}.

Both of the models used by Jenkins (1991) and Hellmer and Jacobs (1995), are likely to overestimate the impact of warmer temperatures at the ice front. This occurs because both models in effect warm all of the ocean cavity with the full amount of warming at the ice front. In contrast, it is expected that in a three-dimensional model the effect of warming will be reduced by the cavity circulation exporting some of the additional heat at depths that do not interact with the ice shelf, and by the internal circulation diluting the impact of the ice front warming.

Grosfeld and Gerdes (1998) considered two possible climate change scenarios, and their impact on the ocean circulation and the ice shelf basal mass balance, using the three-dimensional coupled open ocean and cavity model of Grosfeld et al. (1997). Their model domain included the Filchner Trough, and the ocean cavity under the Filchner Ice Shelf. The two climate change scenarios they examined were (i) an increase in ocean temperatures, and (ii) a reduction in sea ice formation rates in the open ocean part of their model domain. Grosfeld and Gerdes suggested that the reduction in sea ice was the more likely of the two scenarios. They suggested that warm waters, for example, Circumpolar Deep Water (CDW), would be unable to directly access the continental shelf and interact with the ice shelves in the Weddell Sea, while sea ice retreat over the continental shelves due to climate change would reduce the production of HSSW, leading to a reduction in the ventilation of sub–ice shelf cavities. This led Grosfeld and Gerdes to conclude that the immediate response to climate warming would be a thickening of ice shelves around Antarctica, because the reduced sea ice scenario led to a decrease in the melt rate of 0.06 m yr^{-1}.

However, this scenario neglects the deeper ocean warming that could be expected to accompany the reduction in sea ice formation, as found in coupled climate models (e.g., Hirst 1999). As we shall discuss, modeling also shows a reduction in deep convective mixing at high southern latitudes (Hirst 1999) associated with freshening of near-surface waters and warming below about 150 m, while salinities below about 300 m show slight increases. While coupled atmosphere–ocean climate models do not currently have the resolution to accurately describe continental shelf processes, it seems plausible that such a reduced sea ice scenario, with less brine rejection, and decreased production of dense HSSW over the continental shelf, would enable water masses with properties closer to CDW, which is warmer and saltier than HSSW but has a similar density, to intrude onto the shelf. This could occur because the processes that lead to a reduction in HSSW may also lead to changes in the properties of Modified Circumpolar Deep Water (MCDW), which is already present on the continental slope. Using observed properties from the Prydz Bay region (Wong et al. 1998) for HSSW and CDW suggests the magnitude of such a change could eventually lead to warming of up to 3°C. Thus the presence of CDW off the slope, and the possibility that it may move toward the coast suggests an upper limit of 3°C for warming of shelf water masses, without having to wait for the global ocean to warm appreciably at depth.

Here we consider the response of the circulation beneath the Amery Ice Shelf and the ice–ocean interaction to several different climate change scenarios. The changes in the ocean climate are introduced by modifying the ocean temperature field along the northern boundary of the ice shelf cavity. The global climate simulations discussed in section 2 suggest that an ocean temperature warming of approximately 2°C at depths relevant to the flow into sub–ice shelf cavities could be reached by the time atmospheric CO_2 levels reached 3 times preindustrial values. This would occur at about

the end of the twenty-first century under the Intergovernmental Panel on Climate Change (IPCC) IS92A greenhouse scenario (Leggett et al. 1992). Since the warming will arise gradually, since there are uncertainties associated with the climate simulations, and since ocean warming is expected to continue for hundreds of years even if atmospheric CO_2 levels are stabilized, it is useful to consider a range of warming scenarios. Additionally we wish our study to be of use for climate change studies on other timescales, so we present results for temperature increases of 0.25°, 0.5°, 1.0°, 1.5°, 2.0°, and 3.0°C (section 5). These can be considered as sensitivity studies of the ocean circulation and ice shelf basal exchange processes.

Several of the climate change scenarios presented here were previously discussed briefly by Williams et al. (1998b) and were further explored in Williams (1999). The differences between the results presented here and those studies follow from a change in the ice shelf–ocean boundary conditions for the exchange of heat and salt (by the freezing or melting of ice at the interface). Here the boundary conditions at the ice–ocean interface are more sophisticated, with the previous parameterization being replaced by a description based on the three-equation formulation described by Holland and Jenkins (1999). These boundary conditions have also increased the stability of the model for warmer scenarios, allowing the use of a more appropriate mass transport condition at the ice front.

Additionally, there is a change in the tracer (temperature and salinity) boundary conditions at the ice front between Williams et al. (1998b) and the present study. The tracer boundary conditions used by Williams et al. (1998b) were similar to those used here, but contained additional restoration terms. These terms applied restoring toward the tracer boundary data on the outflowing water masses in addition to the inflowing water masses. This effect may not be significant in simulations of the present climate, where it could be considered to constrain the outflow to the observations, but restoring on outflow effectively allows heat and salt to move against the direction of flow and its impact in climate change scenarios could be both large and undesirable.

2. Estimates of ocean climate change

Estimates of likely ocean temperature changes near the Amery Ice Shelf can be taken from modeling studies of various climate change scenarios. The studies discussed here (Manabe and Stouffer 1994; Hirst et al. 1996; Hirst 1999) use fully coupled ocean–atmosphere general circulation models, and consider the effects of increases in the concentration of atmospheric CO_2.

Manabe and Stouffer (1994) looked at two different climate change scenarios, a doubling of atmospheric CO_2 concentration, and a fourfold increase in CO_2 concentration ($4 \times CO_2$), in addition to a control run (no change in the atmospheric CO_2 concentration). In both runs where the CO_2 concentration changed it was increased at the rate of 1% yr^{-1}, until the target value was reached, and then held constant for the remainder of the 500-yr run. This led to a doubling in CO_2 after 70 yr and a fourfold increase after 140 yr. The impact on the ocean temperature field was greater in the fourfold increase study, than in the doubling of CO_2 run.

Several different ocean temperature fields featuring the $4 \times CO_2$ run and the control run were presented by Manabe and Stouffer (1994). They show the latitude–depth distribution of the zonally averaged mean temperature in the Atlantic and Pacific Oceans, for both the model initial conditions and for the average over the 400–500-yr period of the $4 \times CO_2$ run. Comparison between the initial conditions and the $4 \times CO_2$ run provides an estimate of long-term temperature change. Comparison of sea surface temperatures for two time periods were shown: an average for the 130–150-yr period (approximately when the fourfold increase in CO_2 concentration was reached), and an average for the 400–500-yr period. Their figures, respectively, show sea surface temperature differences of ~0° and ~2°C, on the Antarctic coast at the longitude of the Amery Ice Shelf (72°E), demonstrating the long response times of the ocean to changes in forcing. Manabe and Stouffer also presented the zonally and time-averaged mean temperature difference between the $4 \times CO_2$ and control runs for the 400–500-yr period. At the latitude of the front of the Amery Ice Shelf (69°S) and at depths appropriate to ocean exchange with the ice shelf cavity, the temperature change was ~3°C.

Another transient response simulation was carried out by Hirst et al. (1996) using the IS92A CO_2 emissions scenario of Leggett et al. (1992) as forcing for a coupled model that included the Gent and McWilliams (1990) parameterization for eddy mixing in the ocean. O'Farrell et al. (1997) argued that this provides a better estimate of ocean heat uptake and more realistic rates of warming in the ocean adjacent to the ice shelves. The IS92A scenario may also be regarded as a more realistic growth rate for atmospheric CO_2, with doubling of CO_2 concentration in 129 yr, instead of 70 yr as occurs in the 1% yr^{-1} compounding scenario. This simulation was continued to a trebling of CO_2 levels, which was reached after a further 52 yr.

In O'Farrell et al. (1997) ocean temperature anomaly fields based on the results of Hirst et al. (1996) were presented. O'Farrell et al. used these ocean temperature anomaly fields (along with corresponding atmospheric forcing reflecting the increase in precipitation as the climate warms) to drive a model of the Antarctic ice sheet, including the major ice shelves, to study the climate change impacts. A very simple ice shelf basal melting prescription was used. It was based on the temperature changes in the adjacent ocean, and melt rates from laboratory experiments (Russell-Head 1980) and observations of icebergs melting (Hamley and Budd 1986), which are discussed later. Figure 1 based on Fig. 2d of O'Farrell et al. shows the ocean temperature anomaly below 100 m

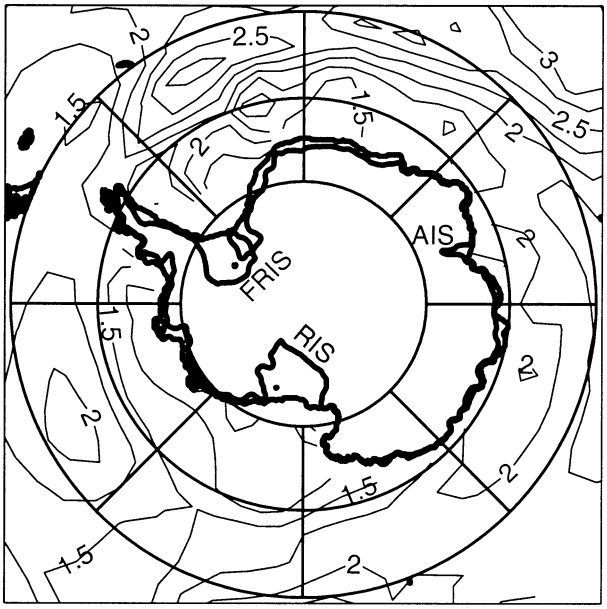

FIG. 1. Mean ocean temperature anomaly field below 100 m, at the time of reaching $3 \times CO_2$ concentration, from the coupled global climate model described by Hirst et al. (1996). Contour intervals are 0.25°C. The locations of the Amery (AIS), Ross (RIS), and Filchner–Ronne (FRIS) ice shelves are indicated. Prydz Bay is adjacent to the Amery ice front as discussed in the text. [From the same anomaly field as portrayed in Fig. 2d of O'Farrell et al. (1997).]

(centered on 250-m depth) from the Hirst et al. simulations at the time when the trebled CO_2 concentration level was reached. This temperature anomaly field, which O'Farrell et al. report has a similar pattern to the anomaly for the 250–750-m ocean model layer, provides a good estimate of the temperature anomaly near the Amery Ice Shelf, because unlike sea surface temperature estimates, this temperature field is at depths where exchange can occur with the ocean cavity under the Amery Ice Shelf. A suitable estimate of the regional temperature change from Fig. 1 would be in the range of 2.0°–2.4°C.

In addition to the changes in temperature we can expect increased precipitation at high southern latitudes in a warmer climate regime, but this is unlikely to counter the increases in ocean temperatures and salinities at the sub–ice shelf depths discussed previously. The freshening of surface waters contributes to reduced deep mixing by impeding the formation of sufficiently dense water by sea ice growth. Modeling shows that a decreasing proportion of the diminishing sea ice cover originates from ocean freezing, compared to an increased snowfall contribution, which also implies diminished brine rejection. Budd and Wu (1998) report that an approximately 25% increase in the excess of precipitation over evaporation occurs over the sea ice zone for the same model run discussed by Hirst et al. (1996), once the tripling of the CO_2 concentration is passed. In a continuation of the same simulations Hirst (1999) has also shown that for waters near the Antarctic margins the surface mixed layer freshens, while below ~400 m the salinity increases by 0.1 psu or more by the time temperature increases of 2°–3°C occur, around 300 yr after the tripling of the CO_2 concentration is reached.

There are several uncertainties associated with these coupled model predictions of warming, including the absence of coupling between the ocean and the Antarctic ice sheet, which eliminates any possible feedback from melting ice shelves. Also the results of transient models (e.g., Manabe and Stouffer 1994; Hirst 1999) indicate ocean temperatures will continue to rise for hundreds of years even if the atmospheric climate forcing is stabilized. Also, as discussed in the introduction, these global models do not resolve the continental shelf and its processes, forcing us to rely on physically motivated arguments to suggest how events there would follow the larger picture. To cover these uncertainties several simulations of the sub–ice shelf ocean conditions were made for different degrees of warming for the water at the ice shelf cavity front. In view of these uncertainties and the transit time for ice passing through the ice shelf—about 600 yr from the grounding line to the ice front—all the simulations were carried out using a sub–ice shelf ocean cavity defined using the present ice shelf geometry. This also allows estimates of the effect of warming on shorter timescales than those over which large changes are expected. This is of some importance since, as will become evident, the larger changes in ocean temperature could lead to substantial modifications of ice shelf geometry, the explicit analysis of which is beyond this current study.

3. Model description

For this study we are using the three-dimensional ocean model for cavities under ice shelves introduced by Determann and Gerdes (1994). The model has since been fully described by Gerdes et al. (1999). The model is a rigid lid, hydrostatic three-dimensional, primitive equation model in σ coordinates, where σ equals the depth below the ice shelf base divided by the water column thickness. The advantage of using σ coordinates in ocean cavity models is that they allow for convenient specification of boundary conditions at the ocean interfaces with the ice shelf and the seabed (these are the top and bottom model coordinate surfaces, respectively). The model derives the horizontal velocity components, potential temperature, and salinity. Vertical velocity is calculated from the continuity equation for an incompressible fluid. Subgrid-scale mixing processes within the water column are parameterized using a conventional eddy viscosity–diffusivity formulation with constant coefficients.

The shape of the ocean cavity under the ice shelf is characterized by the present ice shelf draft and water column thickness (Fig. 2). These are identical to those used by Williams et al. (2001) where details of their deviation are given.

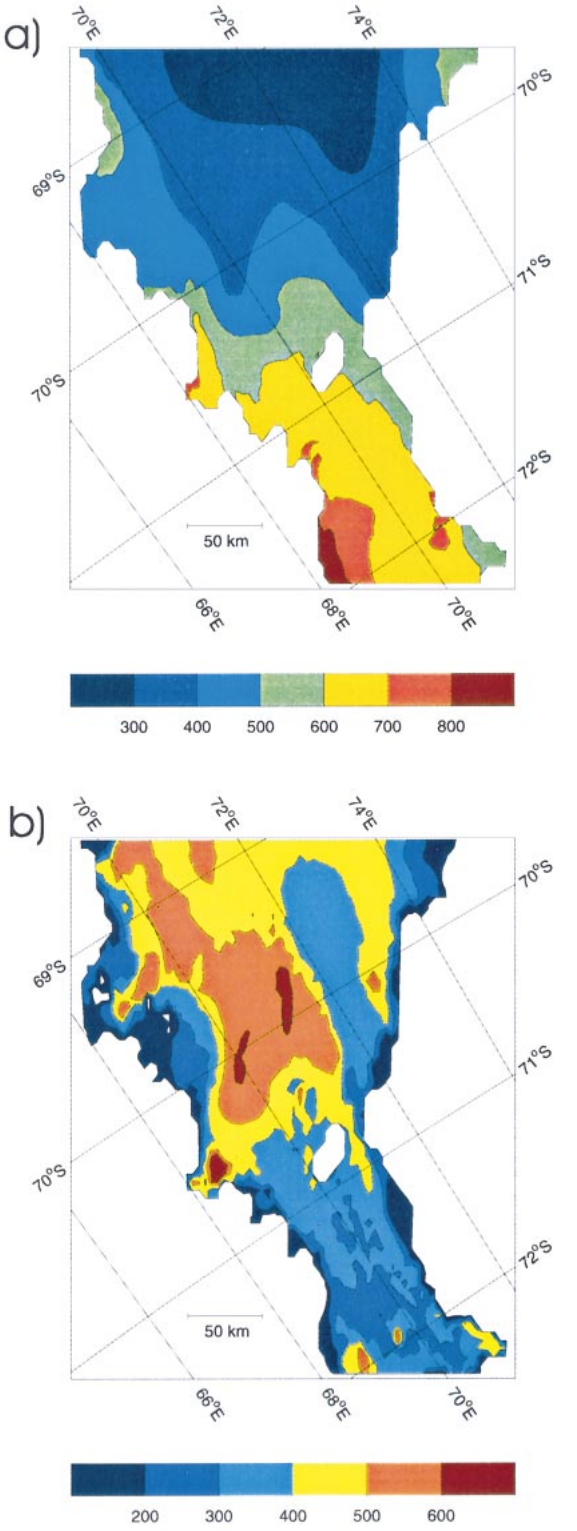

FIG. 2. (a) Ice shelf draft (m) and (b) water column thickness (m) beneath the AIS.

The boundary conditions at the ice front are also identical to those used by Williams et al. (2001), and the baroclinic velocity and tracer terms are based on Stevens (1990). The barotropic velocities in the model are found from the horizontal derivatives of the streamfunction, which represents the external mode in this rigid lid model (Gerdes et al. 1999); hence, the barotropic mass exchange at the ice front can be set (and indeed is required to be set) by prescribing the streamfunction along the ice front. Here we prescribe the same streamfunction at the ice front, and in the same manner, as in the ''specified barotropic exchange'' model run in Williams et al. (2001). This streamfunction is used for all of the model runs in this study (Fig. 3a). It drives approximately 0.7 Sv (1 Sv $= 10^6$ m^3 s^{-1}) of barotropic exchange, with inflow on the eastern side (negative streamfunction gradient with longitude) of the domain and outflow on the western side of the domain (positive streamfunction gradient). It is based on the thermal wind equation and conservation of mass constraints applied to the observed temperature and salinity data available near the ice front (see Fig. 3). Full details of the derivation are given in Williams et al. (2001). It should be noted that the method is similar to that used by Wong et al. (1998) in their oceanographic analysis of heat and freshwater exchanges under the Amery Ice Shelf.

The barotropic flow at the ice front is not uniquely determined by such a procedure, and specifying the streamfunction at an open boundary can potentially introduce some unrealistic flow features. In their study using the same domain and boundary streamfunction, Williams et al. (2001) found some indications of possible inconsistencies between the internal circulation and the prescribed cross-boundary flow. For example, as can be seen in Figs. 4a and 4b in the present study, the western boundary current inside the domain was redirected along the ice front by the prescribed absence of barotropic outflow in that region of the boundary. This effect, however, appears primarily limited to only a few grid points in the northwest corner of the domain, and does not appear to greatly affect the circulation in the remainder of the cavity. This gives us some confidence in the use of this barotropic transport boundary condition. It should also be noted that for this type of domain we are limited in how we are able to treat the streamfunction at the open boundary, as we are unable to use either a simplification of the governing equation (as is done for the baroclinic motion) or the Sverdrup balance argument used for such boundaries in the open ocean (Stevens 1990).

There are versions of this ocean model that couple the adjacent ocean to the sub–ice cavity (Grosfeld et al. 1997; Grosfeld and Gerdes 1998), which avoids the necessity of prescribing the mass transport across the ice front. Some studies coupling the Amery Ice Shelf cavity to the adjacent Prydz Bay region have been carried out (Williams 1999), but these simulations do not presently provide a close enough match to the observed water

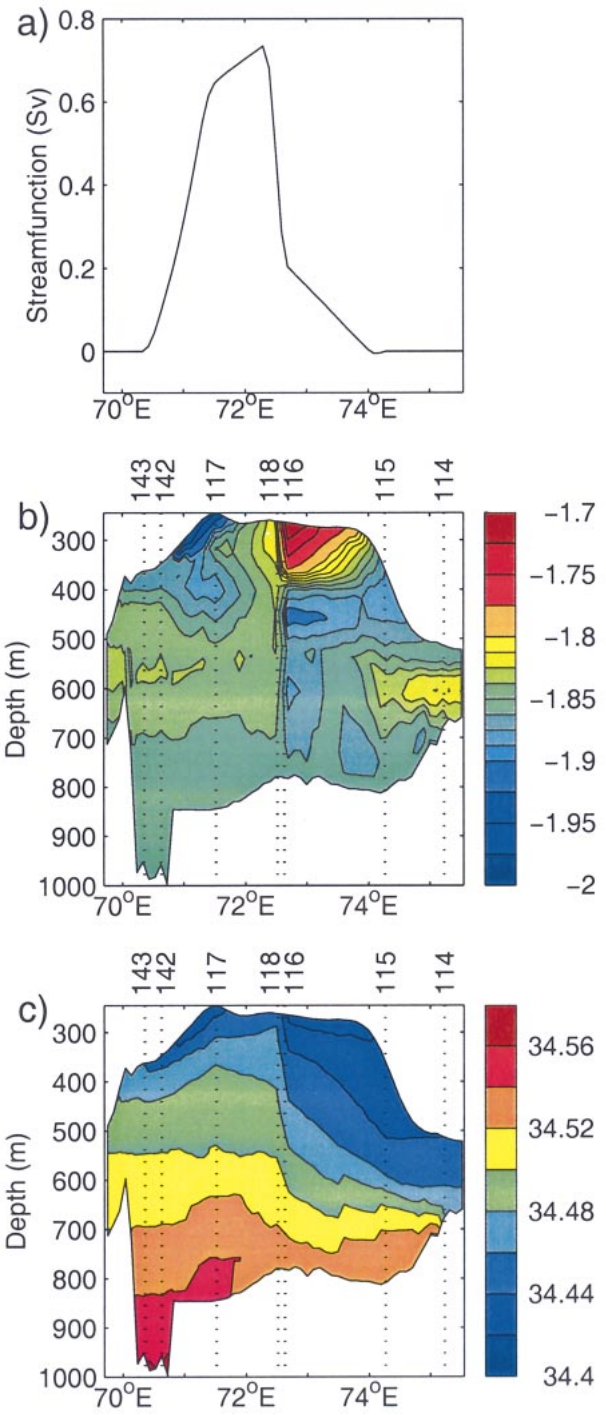

FIG. 3. (a) The streamfunction (Sv), (b) potential temperature (°C), and (c) salinity (psu) specified as boundary conditions along the ice front. The dotted lines mark the locations of the numbered FISHOG hydrographic casts.

masses adjacent to the ice front for them to be regarded as useful for studies of the present circulation regime or for climate change studies.

The tracer boundary conditions follow Stevens (1990), so in areas of inflow on the boundary, tracers are restored with a relaxation timescale of 80 days to a tracer field derived from data collected as part of the FISHOG program (Wong et al. 1998; Figs. 3b,c). The locations of the FISHOG hydrographic stations used are indicated on the figure. Some of the data was obtained at some distance away from the ice front and mapping it to the model boundary can change the horizontal scale of some features in the tracer distributions. This potentially introduces further uncertainties in calculating the streamfunction, but these are unlikely to significantly affect the main model results. In areas of outflow a radiation condition is used that allows tracer properties to be exported from the domain.

The treatment of the coupling of fluxes of heat and salt at the ice–ocean interface differs from those used in previous applications of this model. Here we replace the parameterization described by Gerdes et al. (1999) with a simplified application of the three-equation formulation described by Holland and Jenkins (1999). We do not consider the impact of the buoyancy flux at the ice–ocean interface, instead we use the parameterization of Jenkins (1991) for the turbulence in the boundary layer. This involves a turbulence parameter that is dependent on a friction velocity, and is calculated from the top level cavity velocities following Holland and Jenkins. For completeness we present the equations used to model the ice–ocean interaction in the appendix.

Notable features of this formulation are the inclusion of different molecular diffusion rates for heat and salt in a thin viscous sublayer at the ice–ocean interface, and the distinction between melting and freezing regions in the heat flux part of the energy balance at the ice–ocean interface. In implementing the boundary condition it is assumed that the vertical temperature in the ice shelf is in steady state and that the vertical advection in the ice shelf is implied by the basal rates of melting and freezing. Under these conditions melting steepens the gradient of the temperature in the ice shelf near its base increasing the heat flux into the ice shelf, while freezing forms a layer of ice with a temperature close to the in situ freezing temperature that allows the heat flux into the ice shelf to be ignored in regions of accretion.

For the present application the model comprises 10 σ layers, with layer thicknesses varying from ~2% of the water column thickness in the top layer, to ~23% of the water column thickness in the bottom layer. In the horizontal coordinates we use a latitude–longitude grid rotated by 12° to the east to allow the ice front boundary at Prydz Bay to lie parallel to the model coordinate system. In the rotated domain the horizontal resolution is 0.05° by 0.1°, giving an approximate resolution of 5.5 by 4.3 km.

4. Present conditions under the Amery Ice Shelf

The current oceanographic conditions under the Amery Ice Shelf have recently been discussed by Wil-

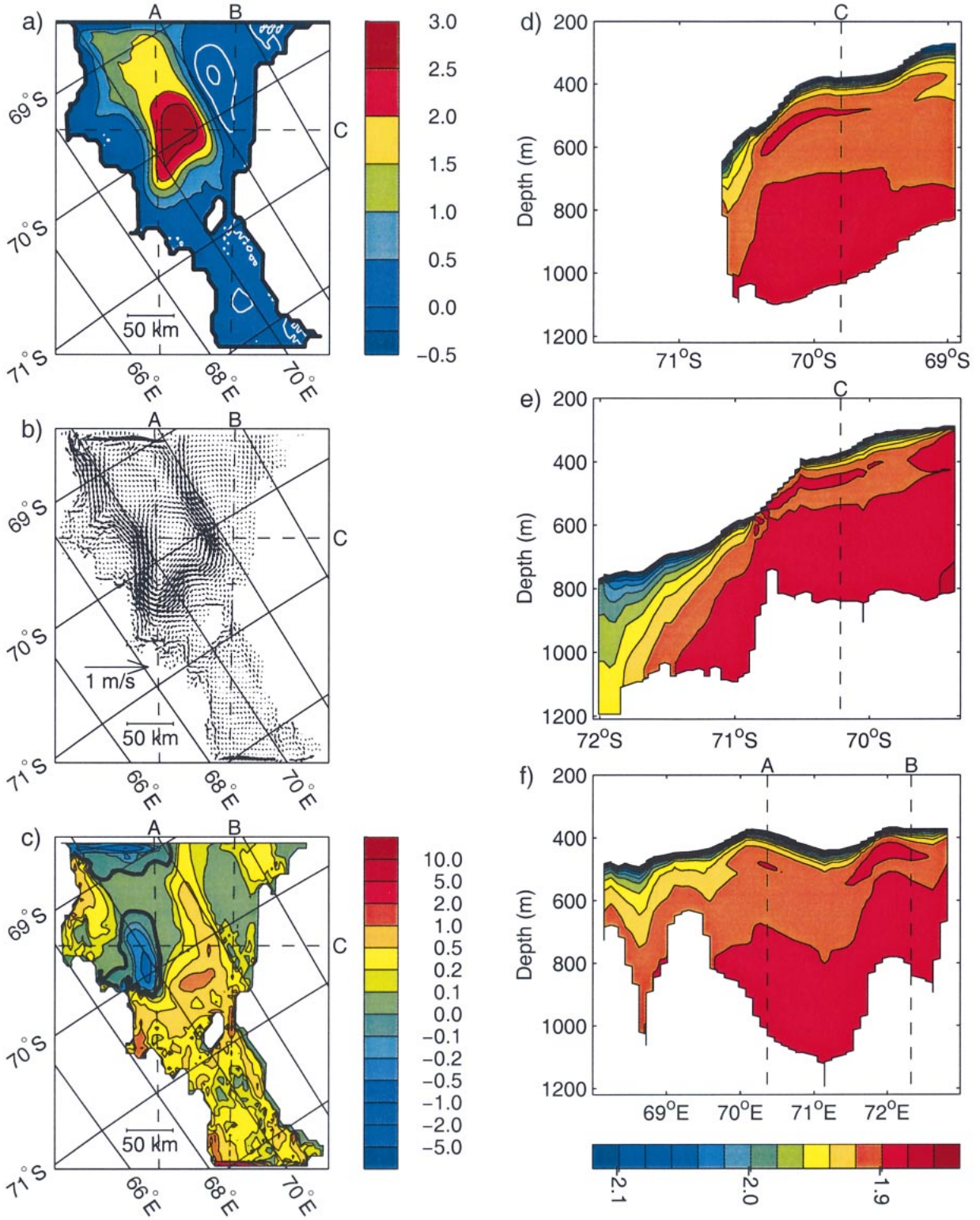

FIG. 4. Results from the AIS_{pres} run. (a) The vertically integrated streamfunction (Ψ), with contour intervals of 0.5 Sv for $\Psi > 0$ (black) and 0.25 Sv for $\Psi \leq 0$ (white). Circulation is clockwise about positive features. (b) The horizontal velocities on the top σ level. (c) The rates of melting (+) and freezing (−) at the ice–ocean interface (m yr^{-1}). The bold contour denotes the boundary between melting and freezing. (d) The potential temperature (°C) along section A. (e) The potential temperature (°C) along section B. (f) The potential temperature (°C) along section C. The same temperature scale (base of right-hand column) is used in (d), (e), and (f). The locations of the sections are indicated by the dotted lines in (a), (b), and (c). The dotted lines in (d), (e), and (f) indicate where the sections intersect.

liams et al. (2001). They investigated two different possible versions of the barotropic boundary condition at the ice front. We have assessed the boundary conditions used by Williams et al. (2001) and found their specified barotropic exchange at the ice front outlined in the preceding section to be the most suitable boundary condition for warming studies.

This treatment differs from the two previous three-dimensional ocean modeling studies that have evaluated the effects of ocean warming on the Amery Ice Shelf. In both Williams et al. (1998b) and Williams (1999) only limited barotropic exchange was allowed at the ice front. This involved the use of an unconventional boundary condition for the streamfunction at the open face of the cavity that allowed some evolution in the barotropic transport across the ice front with increasing ocean warming. In Williams et al. (2001) and the present study this was replaced with a more conventional fixed barotropic exchange boundary condition. [See Williams (1999) for a full discussion of possible ice front boundary conditions.] The preliminary studies of Williams (1999) incorporating the circulation of the adjacent open ocean suggest that the barotropic exchange specified in the present study, as inferred from observed hydrographic data, is more appropriate in its general pattern than the imposition of zero barotropic transport. One reason for the change to a more conventional open ocean boundary condition for the mass transport is the introduction of an improved boundary condition at the ice–ocean interface as discussed in the previous section and detailed in the appendix. In addition to better describing the exchanges at the ice–ocean interface it also enhances model stability compared with previous formulations.

The introduction of the new ice shelf–ocean boundary condition leads to slight modifications in the results presented here for the present ocean climate, compared to previous studies (Williams 1999; Williams et al. 2001). Before presenting the results for the warming scenarios, a description of the present regime under the Amery Ice Shelf is presented. For convenience this model run has been labeled AIS_{pres}.

In sub–ice shelf simulations with this model it has been found that the velocity field is nearly barotropic and is well described by the vertically integrated streamfunction (e.g., Determann and Gerdes 1994; Gerdes et al. 1999; Williams et al. 2001). The main feature of the circulation in the model run for the present climate (Fig. 4a) is the strong, ~2.8-Sv clockwise circulation called the main gyre (70.0°S, 71.0°E), which accounts for most of the meridional transport in the model. It is positioned where the water column is thickest (Fig. 2b). The streamfunction as specified at the ice front (Fig. 3a) restricts inflow across this boundary to a limited area, between approximately 72.5° and 74.0°E. Most of this flow goes south into the main gyre. From there a small amount is pushed south in the channel to the east of the central grounded zone (70.7°S, 70.4°E). The bulk of the flow turns to the west to flow along the western boundary and either recirculates in the main gyre or flows out of the domain around 71.0°E. This last feature of the flow is partly caused by the fixed prescription of the streamfunction along the ice front as discussed in section 3.

The transport in the remainder of the domain is weaker than that in the main gyre. East of 72.0°E the flow in the cavity under the ice shelf is characterized by a weak, topographically trapped, anticyclonic northeastern gyre. South of the main gyre there are two features of note: a complex flow around the central grounded zone, which is coupled to the main gyre, and farther to the south an anticyclonic southern gyre centered at 71.6°S, 69.8°E.

The ocean circulation under the ice shelf is strongly linked to the forcing provided by the ice shelf and the bathymetry. The strength of the interaction between the ice shelf and the ocean can be characterized by the rates of melting and freezing at the interface between the ice shelf and the ocean (Fig. 4c). Where melting occurs, the top of the water column is cooled and freshened, which tends to stratify the top of the water column; and where freezing occurs, salt is released, which tends to drive convective mixing. As we discuss below, both of these tendencies can be overtaken by the effects of the horizontal circulation.

The highest rates of melting occur, as might be expected, in the southeast and southwest of the domain where the ice shelf is thickest. High rates of melting also occur in areas where the ice shelf draft is not the determining factor. In these areas (e.g., around 73.2°S, 70.8°E) horizontally advected water comes into contact with a thickening ice shelf. Here, as can be seen by comparing the currents in the top layer of the model (Fig. 4b) with Fig. 2a, the steep ice shelf draft gradients then drive the water downslope where it is able to drive melting because of the increased temperature difference between the water and the ice shelf. The temperature difference is increased in downslope flow conditions, because the ice–ocean interface, which is at the in situ freezing temperature, gets colder with increased pressure.

The areas of freezing are highly dependent on the underlying horizontal circulation. The two extensive regions of freezing, in the northwest corner of the domain, and around 69.8°S, 69.9°E (Fig. 4c), are in areas where water that has been cooled and freshened by melting at depth is rising in contact with the ice shelf. The strong freezing adjacent to the ice front is partly caused by the redirection of flow along the ice front (see Fig. 4b) by the boundary conditions as discussed in section 3. This enhances the freezing process by directing strong upslope flow.

Integrating the rates of melting and freezing at the ice–ocean interface also allows the mass balance of the base of the ice shelf to be calculated. The results of these calculations are shown in Table 1, where the rates in the first three columns are the area-averaged rates for

TABLE 1. Estimates of the mass balance rates at the base of the Amery Ice Shelf. The total area of the ice shelf is 5.6×10^4 km^2.

	Mean rates				Mass change rates from:		
	Freezing (m yr^{-1})	Melting (m yr^{-1})	Total (m yr^{-1})	Area of melt (%)	Freezing (Gt yr^{-1})	Melting (Gt yr^{-1})	Net (Gt yr^{-1})
AIS_{pres}	0.18	0.34	0.28	87.6	1.1	15.3	14.2
$AIS_{+0.25°C}$	0.22	0.53	0.45	89.5	1.2	24.2	23.0
$AIS_{+0.5°C}$	0.26	0.67	0.58	88.8	1.5	31.1	29.6
$AIS_{+1.0°C}$	0.29	0.90	0.77	89.3	1.6	41.0	39.4
$AIS_{+1.5°C}$	0.32	1.20	1.06	90.4	1.6	55.4	53.8
$AIS_{+2.0°C}$	0.38	1.56	1.40	91.9	1.6	72.9	71.3
$AIS_{US+1.0°C}$	0.29	0.90	0.77	88.5	1.7	40.8	39.1
$AIS_{US+2.0°C}$	0.41	1.57	1.40	91.4	1.8	73.4	71.6
$AIS_{US+3.0°C}$	0.53	2.08	1.90	93.1	1.9	98.8	96.9
AIS_{cool}	0.16	0.30	0.23	85.6	1.2	13.1	11.9
AIS_{cold}	0.10	0.17	0.11	76.6	1.2	6.6	5.4

regions where freezing or melting occur, and for the total ice shelf area. The next column contains the percentage area of the ice shelf where melting is occurring. The remaining columns show the mass gain from freezing, mass loss from melting, and the net mass loss from the ice shelf. For the AIS_{pres} model run the net mass loss from the ice shelf is 14.2 Gt yr^{-1}. This agrees well with oceanographic observational estimates by Wong et al. (1998) that indicate a mass loss ranging between 10.7 and 21.9 Gt yr^{-1}, with a preferred mean of 14.7 Gt yr^{-1}.

The local change in temperature levels shows the localized movement of water masses. In areas of strong melting, a cold and fresh meltwater layer forms at the top of the water column. This is then advected away from the melting area by the general horizontal circulation, or rises as a ''plumelike'' feature up the base of the ice shelf. The latter behavior can be seen in Fig. 4b on the western side of the southern part of the domain at approximately 70.5°S, 69.0°E. These processes allow warm water to upwell and continue driving the melting. In areas of high melt this leads to increased stratification in the density field.

In contrast, areas of freezing can lead to a more vertically homogeneous water column, as salt is rejected into the top of the water column. Unless it is advected away by currents in the upper levels this saltier water drives strong overturning, which leads to weak vertical density gradients. The effect of these processes on the water column can be seen in three temperature sections through the model domain. These sections, whose locations are indicated in Figs. 4a–c, are labeled A, B, and C.

Section A (Fig. 4d) shows a typical temperature structure on the western side of the main gyre. Adjacent to the ice shelf base is a highly stratified region that is formed by the interaction at the ice–ocean interface. This stratified layer tends to thicken to the north with the strong freezing near the ice front driving vertical mixing. The mixing depth is limited by continual replacement of the water column by the horizontal transport. The relatively thick layer of water at ~ -1.95°C at the southern end of the section is a combination of local melting cooling the water, and the advection into this region of meltwater formed to the south of the central grounded zone.

In the remainder of this section the stratified layer tends to be thin as the strong velocities in the main gyre cause a rapid replacement of the water in the top layers near the ice shelf, both along and across the northern part of the section. Below this the temperature is weakly stratified in two layers. The warmest water (~ -1.89°C) in the model domain fills the lower portion of the water column and above that lies a broad layer of slightly cooler water (~ -1.91°C). In the middle of that cooler layer is a pocket of warmer water that is being transported by the main gyre. This pocket can also be seen in the other two sections. It is the signature of a warm patch in the temperature specified along the ice front (Fig. 3b; 73.0°E). This warm patch originates in the inflow region, so its signature is transported into the model domain. The structure around this warm pocket remains stable because of the dominant role the salinity field has in setting the density gradient for these temperatures.

The structure of the temperature in the northern part of section B (Fig. 4e) is similar to that seen in section A, but with two small variations. Over most of the section, the layer containing the pocket of warmer water in the middle of the water column is thinner. At the northern end of the section, near the ice front, the inflow across the boundary has led to a water column that is well mixed except for a small amount of stratification at the top that is maintained by interaction with the ice shelf.

The southern end of this section shows the effects of strong melting in conjunction with internal mixing and weak horizontal transport. This combination has led to a fairly evenly stratified water column with a reduced temperature gradient adjacent to the ice shelf. The isotherms close to the southern boundary indicate water near the ice shelf is upwelling to supply heat for melting.

Section C (Fig. 4f) runs east–west, and it highlights

features of the circulation not seen in the other two sections. In the area of the main gyre (approximately 69.5°–72.0°E), the water being transported south on the eastern side of the gyre is warmer and better mixed than the northbound water on the western side of the gyre. On both sides of the gyre the vertical temperature structures that might have been anticipated from simple considerations of local melting or freezing do not occur. On the eastern side of the gyre (~71.5°E) where melt rates of up to 1.0 m yr^{-1} are found, no significant meltwater layer forms while the layer of meltwater on the western side of the gyre also appears unaffected by the relatively high freezing rates (~0.5 m yr^{-1}) in that area. This situation arises due to strong horizontal velocities on the edges of the main gyre, which transport the fresher water formed by melting on the eastern side of the gyre to the western side of the gyre before a meltwater layer can form adjacent to the ice shelf and advect water away from the freezing zone before substantial mixing can occur.

5. Changes resulting from future warming

The different climate change studies discussed in section 2 suggest that with increased atmospheric CO_2 levels, ocean temperatures in the vicinity of the Amery Ice Shelf may eventually change by up to ~3°C near 500-m depth, with a temperature change of around 2°C at depth as the time-tripled CO_2 levels are reached. Smaller increases could be reached much sooner. The studies also suggest that ocean temperature change of this magnitude is unlikely to occur without salinity also changing in the region of the ice shelf front.

At present the formation of sea ice maintains the cold (~−1.9°C) and relatively fresh water (~34.5 psu) found over the continental shelf in Prydz Bay. As discussed previously, the climate change scenarios suggest that reductions in the rate of sea ice formation and reduced deep convection in the Southern Ocean could allow warmer and more saline waters with characteristics closer to CDW, for example, some form of MCDW, to encroach onto the continental shelf in Prydz Bay. However, any initial change in salinity is likely to be very small.

a. Warming scenarios: +0.25° to +2.0°C

Initially we consider only changes in temperature, but as temperature increases the water column becomes less stable. This limits us to considering warming by up to 2.0°C, which we apply additively to the present-day temperatures along the front of the cavity in Prydz Bay. Warming of the water column is expected to be gradual so we investigate warming scenarios for uniform temperature increases of +0.25°, +0.5°, +1.0°, +1.5°, and +2.0°C across the ice front. This also provides us with some sensitivity tests. These runs are labeled $AIS_{+0.25°C}$, $AIS_{+0.5°C}$, $AIS_{+1.0°C}$, $AIS_{+1.5°C}$, and $AIS_{+2.0°C}$, respectively.

TABLE 2. Transport in the main features of the circulation. Positive values indicate clockwise transport.

	Main gyre (Sv)	Northeastern gyre (Sv)	Southern gyre (Sv)
AIS_{pres}	2.85	−0.27	−0.03
$AIS_{+0.25°C}$	3.70	−0.37	−0.08
$AIS_{+0.5°C}$	4.44	−0.42	−0.16
$AIS_{+1.0°C}$	5.46	−0.54	−0.21
$AIS_{+1.5°C}$	6.02	−0.40	−0.44
$AIS_{+2.0°C}$	6.16	−0.07	−0.69
$AIS_{US+1.0°C}$	5.81	−0.42	−0.32
$AIS_{US+2.0°C}$	5.77	−0.27	−0.73
$AIS_{US+3.0°C}$	6.55	−0.22	−0.75
AIS_{cool}	2.60	−0.26	−0.03
AIS_{cold}	1.71	−0.19	−0.02

The increased temperatures along the ice front lead to noticeable changes in the ocean cavity. The internal circulation is strongly affected, the water column becomes on average fresher and warmer, and there is greater melting at the ice–ocean interface.

The strength of the circulation in the main gyre increases monotonically with the warming. This can be seen in Table 2, which shows the transport in the main circulation features. Away from the main gyre the warming has different effects in the north and south of the domain. The anomalies of vertically integrated streamfunctions, referenced to the AIS_{pres} model run, for the $AIS_{+1.0°C}$ (Fig. 5a) and $AIS_{+2.0°C}$ model runs (Fig. 5b) show this clearly.

For warming up to and including 1.0°C the pattern of circulation is largely similar to that found for the AIS_{pres} model run, but with an increase in the strength of the gyres (Table 2). There is also a slight northward shift in the position of the center of the southern gyre. By the $AIS_{+1.0°C}$ run the main and northeastern gyres have approximately doubled their strength, while the southern gyre has dramatically increased compared to the present situation. For the $AIS_{+1.5°C}$ and $AIS_{+2.0°C}$ model runs there are further substantial changes in the circulation. In the north of the domain the northeastern gyre reduces as part of a regional small positive anomaly in model run $AIS_{+2.0°C}$ (Fig. 5b). The main gyre increases again, but less vigorously, while in the south of the domain, the southern gyre increases markedly in strength and size (Table 2). This increases its influence on the flow around the central grounded zone.

At the ice–ocean interface there is an increase in the amount of mass lost from the ice shelf with the increase in temperature. Figures 5d and 5e show the melting and freezing rates over the cavity for the $AIS_{+1.0°C}$ and $AIS_{+2.0°C}$ runs, respectively.

Comparing these figures and the corresponding rates for the AIS_{pres} model run (Fig. 4c) it can be seen that there is a general increase in the rates of melting over

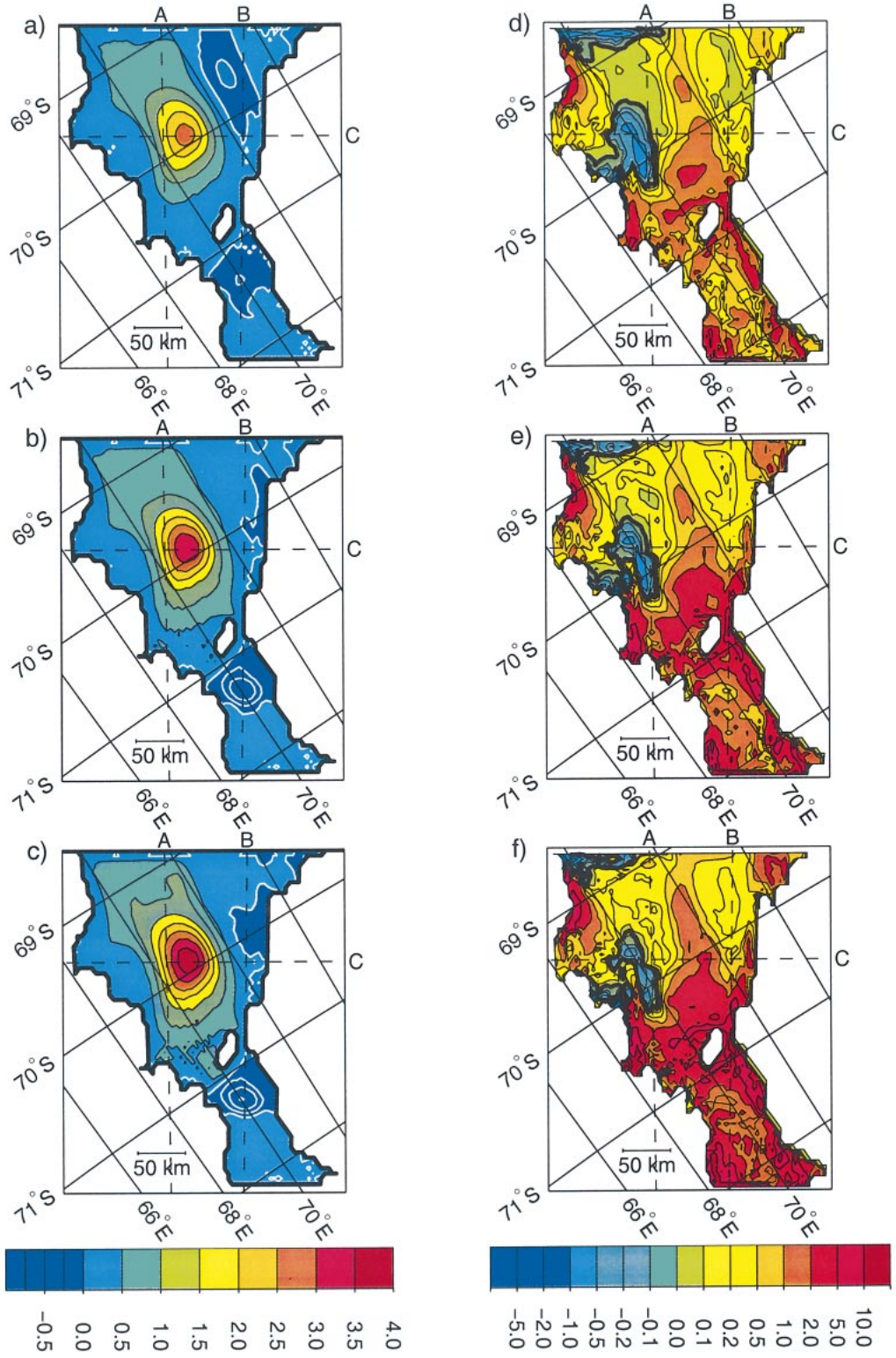

FIG. 5. Anomalies of vertically integrated streamfunctions ($\Delta\Psi$) compared with AIS_{pres} (left color bar, Sv) for the (a) $AIS_{+1.0°C}$, (b) $AIS_{+2.0°C}$, and (c) $AIS_{US+3.0°C}$ model runs, and the rates of melting (+) and freezing (−) at the ice–ocean interface (right color bar, m yr^{-1}) for the (d) $AIS_{+1.0°C}$, (e) $AIS_{+2.0°C}$, and (f) $AIS_{US+3.0°C}$ model runs. Contour intervals for (a), (b), and (c) are 0.5 Sv for $\Delta\Psi > 0$ (black) and 0.1 Sv for $\Delta\Psi \leq 0$ (white), with clockwise circulation about positive features. In (d), (e), and (f) the bold contour denotes the boundary between melting and freezing.

TABLE 3. Extreme tracer values.

	Temperature		Salinity	
	Min (°C)	Max (°C)	Min (psu)	Max (psu)
AIS_{pres}	−2.42	−1.80	34.29	34.52
$AIS_{+0.25°C}$	−2.42	−1.63	34.20	34.51
$AIS_{+0.5°C}$	−2.41	−1.46	34.11	34.47
$AIS_{+1.0°C}$	−2.41	−1.04	33.94	34.48
$AIS_{+1.5°C}$	−2.40	−0.62	33.78	34.41
$AIS_{+2.0°C}$	−2.40	−0.36	33.62	34.39
$AIS_{US+1.0°C}$	−2.42	−1.16	34.25	34.70
$AIS_{US+2.0°C}$	−2.42	−0.29	33.91	34.67
$AIS_{US+3.0°C}$	−2.40	0.63	33.59	34.63
AIS_{cool}	−2.42	−1.90	34.31	34.53
AIS_{cold}	−2.43	−2.07	34.37	34.53

most of the domain. Importantly, it is clear that freezing still occurs at some locations under warmer conditions.

Table 1 shows several measures of the change in the basal component of the ice shelf mass balance. The unexpected feature of the ice shelf–ocean interaction is that although there is a large increase in mass loss from the ice shelf there is also an increase in the amount of ice accreted. This increase in accretion comes from increases in the freezing rates that are large enough to compensate for the decrease in the area of freezing from 12.4% of the ice shelf to 8.1% between the AIS_{pres} and $AIS_{+2.0°C}$ model runs.

Table 3 shows the temperature and salinity ranges within the model domain from the various model runs. The increase in the maximum temperature inside the cavity is clearly associated with the increase in the temperature along the ice front. The minimum temperature in the cavity, controlled by interaction with the deepest parts of the ice shelf, cannot increase significantly. That it does change slightly with warming, highlights the increased temperature gradients that are occurring between the ice–ocean interface and the top layer of the ocean model and the influence that the freshening of the top layer has on the freezing point. This effect can be seen clearly in the temperature along section B in the $AIS_{+1.0°C}$ and $AIS_{+2.0°C}$ model runs (Figs. 6a,b), where adjacent to the ice shelf there is a distinct increase in the number of isotherms. The other noticeable feature in these temperature sections is the increased stratification in the temperature.

The decrease in salinity in the cavity (Table 3) is a direct result of the increased freshwater input from melting at the ice–ocean interface (Table 1) with the largest salinity change in the waters adjacent to the ice shelf. In contrast, the saltiest waters are little changed.

b. *Effect of uniform higher salinity and warming*

Increasing the uniform ocean warming applied to the present-day temperature and salinity fields, which we

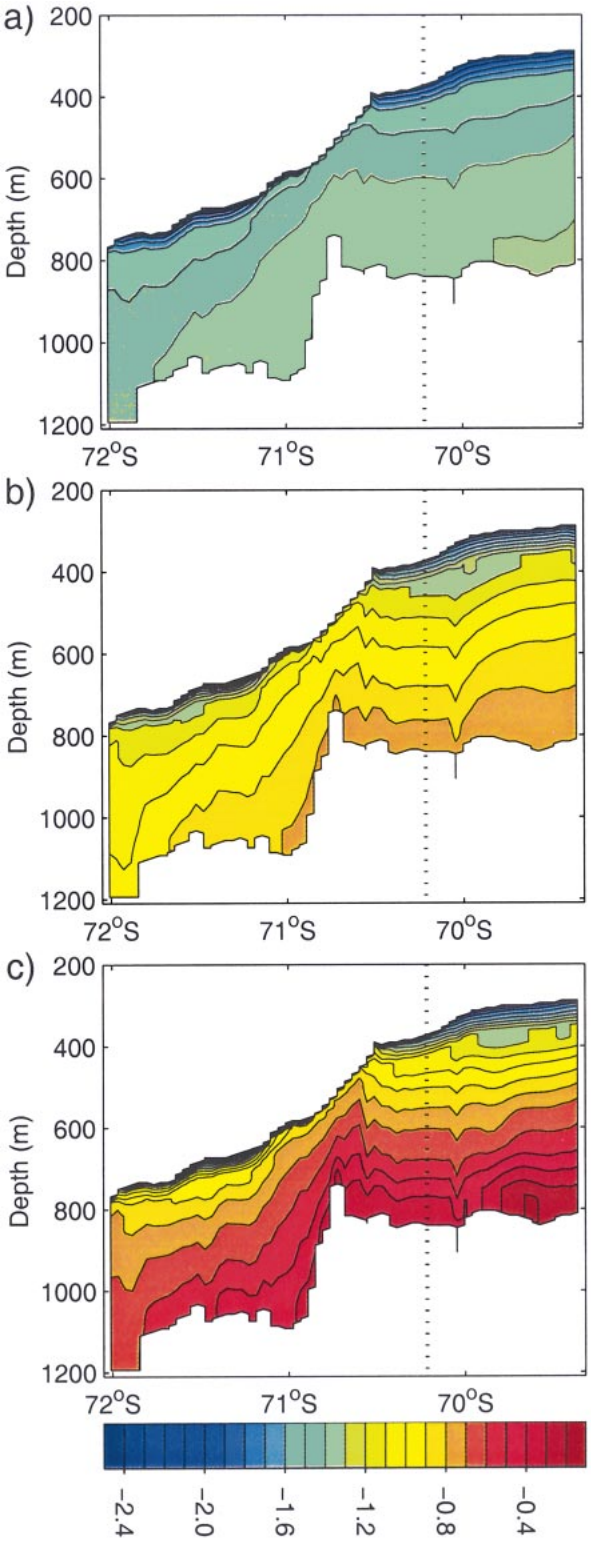

FIG. 6. The potential temperature (°C) along section B for the (a) $AIS_{+1.0°C}$, (b) $AIS_{+2.0°C}$, and (c) $AIS_{US+3.0°C}$ model runs. The location of the section is indicated in Fig. 5. The dotted line indicates the intersection with section C.

prescribe as boundary conditions along the open boundary at the ice front, eventually introduces instabilities in the water column density profiles. These instabilities arise from the nature of the equation of state. At temperatures close to the surface freezing point the density gradient is largely determined by the salinity gradient. However, as temperatures increase by even a few degrees, temperature becomes more important in determining density, while at the same time simply increasing the presently observed temperature distributions probably becomes less valid.

Previously we identified possible future temperature increases along the front of the Amery Ice Shelf by up to 3.0°C. It was also indicated that this amount of warming could be associated with an increase in salinity, as it will likely come from the movement of warmer, saltier water masses, like CDW or MCDW, onto the continental shelf.

Here we present three different model runs with an increased salinity to represent these changes in the character of shelf waters. For simplicity a single uniform high salinity of 34.8 psu is specified for the water outside the cavity. Although this salinity is outside the present salinity range of CDW in the vicinity of Prydz Bay (Wong et al. 1998), it results in reasonable maximum salinities of 34.70 psu or less inside the cavity (Table 3) and is also the minimum value for which the model run would spin up with a temperature increase of 3.0°C applied (for consistency) to the original present temperature distribution, and maintaining the same barotropic mass transport at the open boundary as used throughout the present study.

Accordingly this salinity was used for all three of the uniform salinity model runs ($AIS_{US+1.0°C}$, $AIS_{US+2.0°C}$, and $AIS_{US+3.0°C}$) to provide a consistent salinity forcing at the front of the cavity. This was considered desirable for this warming study as any trends in the model results could then be attributed solely to changes in temperature. In reality the response to climatic warming can be expected to involve an interactive coupling between the cavity and the external domain. This would lead to changes in both tracer and mass transport forcing for the cavity model, but that is beyond the scope of the present study.

Comparisons of the circulations for the pairs of model runs for warming of +1.0° and +2.0°C show some differences, although the circulation patterns for $AIS_{+1.0°C}$ and $AIS_{US+1.0°C}$ are very similar. There are some changes in the strengths of the gyres (see Table 2)—for example, the southern and main gyres are stronger for the $AIS_{US+1.0°C}$ case while the northeastern gyre is weaker. The +2.0°C model runs have an opposite trend, with the main gyre weaker in the $AIS_{US+2.0°C}$ model run (Table 2) than in the $AIS_{+2.0°C}$ run. The other notable change in the $AIS_{US+2.0°C}$ model run is the continued presence of a distinct northeastern gyre with a transport of −0.27 Sv in comparison to −0.07 Sv in the $AIS_{+2.0°C}$ model run. The change in salinity along the ice front between the two +1.0°C warming runs has only a minor effect on the basal mass balance of the ice shelf (Table 1). This is not surprising, since with a fixed barotropic transport into the cavity there will only be minor differences in heat fluxes due to baroclinic differences caused by the difference in the salinity field.

The change to a constant higher salinity at the ice front does have a noticeable effect on the range of temperatures in both the $AIS_{US+1.0°C}$ and $AIS_{US+2.0°C}$ model runs in comparison with the $AIS_{+1.0°C}$ and $AIS_{+2.0°C}$ model runs (Table 3), although there are similarities in the structure of the temperature sections between the two +1.0°C runs. At the ice–ocean interface the change in salinity slightly modifies the temperature, because of the role that salinity has in determining the in situ freezing temperature. There is also an increase in the warmest temperature in the model cavity for both model runs, presumably due to slight (baroclinic) changes in the inflow and outflow at the ice front modifying the temperatures flowing into the model domain.

In the $AIS_{US+1.0°C}$ and $AIS_{US+2.0°C}$ runs the salinities are substantially saltier than in the comparable model runs with the original salinity field (Table 3). The salinities in both of these model runs place the water mass effectively flowing into the model domain as MCDW. This is a water mass currently present on the continental shelf in Prydz Bay, but not observed close to the ice front (Wong et al. 1998). As previously discussed, a possible mechanism for warmer waters to appear on the continental shelves around Antarctica is for CDW to encroach onto the shelf. A reasonable precursor of this would be a decrease in sea ice formation, a reduction in HSSW production, and an increase in the amount of MCDW on the continental shelf.

The pattern of circulation in the $AIS_{US+3.0°C}$ model run is similar to that found in the other model runs, as can be seen from the streamfunction anomaly (Fig. 5c). It shows a generally similar trend in the transport in the gyres to that found for the warmer cases of the initial set of warming runs; namely, a further (smaller) increase in the strength of the circulation in the main gyre and the southern gyre (cf. Fig. 5b), although there is only a slight decrease in the strength of the northeastern gyre compared with the present circulation (see Table 2). A slightly different perspective on the progression is gained by comparing the circulations of the uniform salinity runs.

Increasing the temperature along the ice front by 3.0°C leads to a continued increase in ice loss from the ice shelf. Figure 5f shows that most of the increased loss is coming from a general increase in melt rates over most of the model domain. Accompanying this is a reduction in the area where freezing is occurring, although in areas where freezing still occurs the mean freezing rate increases (Table 1).

In the $AIS_{US+3.0°C}$ model run the effects of the warming at the ice front lead to further temperature stratification in the cavity interior and an increase in the thermal

gradient adjacent to the ice shelf (Fig. 6c). The salinity and temperature ranges (Table 3), however, are consistent with water masses presently found in Prydz Bay. The warmest and saltiest water lies within the broad classification of MCDW and the freshest coldest water is clearly Ice Shelf Water (ISW).

6. Cooling along the ice front

In addition to considering the warming scenarios described above we investigate the possible effects that colder water in Prydz Bay could have on the ocean cavity under the Amery Ice Shelf. Slightly colder water in Prydz Bay may have occurred in the past, perhaps in the recent preindustrial period, or during the Little Ice Age. However, there are limits to how much colder the water could be, depending on the difference between the present water temperatures and either the surface freezing point, or (as an extreme case) the freezing point appropriate to previous interactions with an ice interface at depth. It should be noted that the ice sheet configuration in the Amery region would be considerably different during the Last Glacial Maximum. We examine two colder scenarios. In the first (AIS_{cool}) the water throughout the water column is assumed to be cooled to the surface freezing temperature (~ -1.9°C), except where it is already cooler. This cools the temperatures prescribed in this study along the ice front by a mean value of ~ 0.03°C and a maximum of ~ 0.25°C. In the second scenario (AIS_{cold}), we assume the waters are cooled to the in situ freezing temperature corresponding to the minimum ice shelf draft at the Amery ice front (235 m). This cools the water column by a mean value of ~ 0.20°C and a maximum of ~ 0.43°C.

The circulation is largely unaffected by slightly cooling the cavity. In the AIS_{cool} model run the transport in the gyres does not reduce substantially in strength (Table 2) from the present AIS_{pres} values. In the AIS_{cold} model run the strength of the circulation is weaker but the structure is basically unchanged. There are noticeable changes in the mass loss from the ice shelf as the melting rate decreases over most of the model domain in both model runs (Table 1). This is linked to the cooler water coming into the model domain (Table 3). This also affects the temperature structure, reducing the temperature gradient in the ocean cavity. The cooling of the warmest waters leads to a reduction in the temperature gradient through the water column, and to a generally more homogeneous water column.

7. Discussion and conclusions

The climate change studies with coupled climate models discussed earlier indicate a future rise in ocean temperatures at depths below 200 m, around the Antarctic coast. This motivates our assumption that the ocean will warm in front of the Amery Ice Shelf as global warming proceeds. As a further sensitivity test, and to indicate how far the present situation is from lower limits on ice shelf basal melting, we also considered two colder ocean scenarios.

In the first set of warming scenarios presented here, for oceanic temperature increases of up to 2°C, it was assumed that the salinity along the ocean boundary remained unchanged. For warmer scenarios, and also for repetitions of the $+1.0$° and $+2.0$°C warming scenarios, the salinity was also changed to represent HSSW being mixed with and replaced by MCDW or CDW.

Generally the different climate change scenarios led to similar patterns of circulation in the ocean cavity. The increase in the ocean temperatures tended to expand the extent of the main gyre and the magnitude of the barotropic velocity around its edges also increased. In the southern gyre this expansion was limited to the north by the central grounded zone and to the east and west by the grounding line. Circulation in both these gyres increased considerably (Table 2) with warming, although the incremental increases for greater warming were small, as shown by the similarity of the streamfunction anomalies in Figs. 5b and 5c.

The behavior of the northeastern gyre varied greatly in the different warming scenarios. Initially it increased in strength (doubling by model run $AIS_{+1.0°C}$; Fig. 5a), but with further warming it weakened (model run $AIS_{+2.0°C}$; Fig. 5b).

Two results that might be expected from warming the ocean are an increase in the mean melt rate and a decrease in the mean freezing rate. The first of these occurred in all the warming scenarios, but the second did not. The area of freezing does decrease with increased temperature. This occurs because, where freezing is marginal under present conditions, the introduction of warmer waters can change the area from freezing to melting. This confines the area of freezing largely to regions where freezing was (and remains) substantial, thus increasing the mean freezing rate. This feature of increasing mean accumulation rates from freezing was also seen by Grosfeld and Gerdes (1998) in their climate change scenarios for the Filchner Ice Shelf.

In the warming scenarios the amount of ice lost from the ice shelf increases with increasing temperature. This change comes from increases in both the area of melting and the rate of melting. These combine to give an increase in the total rate of melting. The amount of ice lost and the total melt rate for the ice shelf increase approximately linearly with the change in temperature. This trend is common to both the uniform salinity model runs and the unchanged salinity runs. The mean rates of change for the total melt rates and net ice loss over all the model warming runs are 0.55 m $yr^{-1}°C^{-1}$ and 28.4 Gt $yr^{-1}°C^{-1}$. The largest rate of change is between the AIS_{pres} model run and the $AIS_{+0.25°C}$ model run, with rates of change of 0.68 m $yr^{-1}°C^{-1}$ and 35.2 Gt $yr^{-1}°C^{-1}$. The smallest rates of change are between the AIS_{pres} and the $AIS_{US+1.0°C}$ model run, which has rates of change of 0.49 m $yr^{-1}°C^{-1}$ and 24.9 Gt $yr^{-1}°C^{-1}$. These largest and smallest rates bracket

TABLE 4. Melt rates of fresh ice in ocean water as a function of temperature. After Russell-Head (1980) and Budd et al. (1994).

Temperature (°C)	−1.3	−0.8	−0.3	+0.2	+0.7	+1.2	+1.7	+2.2
Melt rate (m yr^{-1})	2.2	6.6	12.0	18.6	25.6	34.3	43.0	52.6

the general trend and represent the variability associated with the warming trend. Closer inspection of the mass exchange values in Table 1 shows that the change between individual model runs for various levels of warming varies considerably. For example the warming between model runs $AIS_{US+2.0°C}$ and $AIS_{US+3.0°C}$ is 78% of that for warming between $AIS_{US+1.0°C}$ and $AIS_{US+2.0°C}$. Thus, although the general trend is linear, the changes for smaller increments of warming varied noticeably from the mean rate. With the barotropic mass transport prescribed, the mean trend indicates that the increased contrast in temperatures between inflowing waters and the ice shelf base is effective in increasing melting, rather than warmer waters simply being exported after the same heat exchange as before. In a more comprehensive model including the adjacent ocean it is possible that there would also be increased mass transport across the ice front.

The trend of increasing melt rates with ocean warming found here is approximately three-quarters of that found by Grosfeld and Gerdes (1998) for the Filchner Ice Shelf in their first climate change scenario, where they effectively increased the temperature along the northern boundary by 0.6°C. Their temperature increase resulted in a change in the mean rate of melting by ~0.76 m yr^{-1}°C^{-1}.

The trend is also noticeably less than for the plume model of Jenkins (1991) who found a change in melt rate of 3.4 m yr^{-1}°C^{-1}, or the Ross Ice Shelf study of Hellmer and Jacobs (1995) who suggest a sensitivity of 1.2 m yr^{-1}°C^{-1}. The magnitude of the sensitivity to warming in these models in comparison to the sensitivity found in this study is noticeably larger, but both of these simplified models concentrate on particular aspects of the sub–ice shelf circulation in isolation, and as already noted (section 1), both of these models are likely to greatly overestimate the sensitivity of the ice shelf to warming.

The results presented here for the melt rates differ from those in Williams et al. (1998b), where it was found that for present conditions the mean melt rate was 0.16 m yr^{-1}, and the net melting from the ice shelf was 7.8 Gt yr^{-1}, substantially lower than the AIS_{pres} run in this study. The difference is due to the different ice–ocean and ice front boundary conditions, as discussed earlier. The results of Williams et al. (1998b) should not be completely dismissed, as similar responses in the melt rate and net loss rate from the ice shelf to ocean temperature changes were found in that study. For temperature changes of up to +1.0°C, with no changes in salinity the total melt rate changed at ~0.5 m yr^{-1}°C^{-1}, and the net ice loss varied at ~25 Gt yr^{-1}°C^{-1}.

Williams (1999) extended the Williams et al. (1998b) study to include warming scenarios up to 3.0°C. That study also altered the model treatment of ice front boundary conditions to remove the effects of possible upstream advection of heat across the boundary. Over the nine warming scenarios considered by Williams the mean change in the total melt rate was 0.45 m yr^{-1}°C^{-1} and the change in the net ice loss was 22.0 Gt yr^{-1}°C^{-1}. The results and associated uncertainties from these two previous studies have significant overlap with those of the current study. This suggests the change in melting with regard to warming is largely internally determined by the model and not strongly controlled by the parameterizations of the boundary conditions.

Budd et al. (1994) presented a series of melt rates for ice shelves (Table 4). The change in the melt rates with temperature were based on the laboratory studies of Russell-Head (1980) and inferences made from icebergs by Hamley and Budd (1986). The differences in the melt rate with temperature follow a nonlinear trend and are substantially larger than the mean melt rates found in this study. For a temperature increase of 0.5°C the mean melt rate increase with temperature is 7.2 m yr^{-1}. At temperatures close to the seawater surface freezing temperature (~−1.87) the rate of change is 4.4 m yr^{-1} for 0.5°C. For temperature change between 2.5° and 3.0°C above surface freezing (0.7° and 1.2°C) the change in melt rate is larger, at 8.7 m yr^{-1}. The differences in the rates of change of melt rates in response to changes in ocean temperature, between those presented by Budd et al. and the mean melt rate responses presented here, can be attributed to the ability of the ice shelf to protect itself from warm water by forming a layer of meltwater adjacent to the ice shelf. The meltwater layer has temperatures close to the freezing point so melt rates are reduced. A free drifting iceberg, on which the melt rates of Budd et al. are based, is unlikely to be able to form such a protective layer. Under an iceberg any meltwater is likely to rise from the base of the iceberg toward the ocean surface, because the meltwater is relatively fresh and, hence, less dense. This effect has been reported by Russell-Head (1980) and El-Tahan et al. (1987). Under the ice shelf the cooled and freshened water resulting from melting will either rise buoyantly or be transported by the general circulation, but it still remains under the ice shelf, thus effectively protecting another part of the ice shelf downstream of the melting zone. There is also the potential for the melted ice to freeze back on the ice shelf, further reducing the net impact of melting on the ice shelf.

Although the rate of change with temperature presented by Budd et al. is substantially different from the trend presented here for the mean melt rates, there is more similarity with the change in maximum melt rates. The maximum melt rates in the model runs vary between

6.3 m yr^{-1} for the AIS_{pres} run and 33.0 m yr^{-1} for the $AIS_{US+3.0°C}$ run. The increase in the maximum melt rate with warming varies from 8.94 m $yr^{-1}°C^{-1}$, between the AIS_{pres} and $AIS_{US+3.0°C}$ runs, to 11.52 m $yr^{-1}°C^{-1}$, between the AIS_{pres} and $AIS_{+0.25°C}$ runs, with a mean of 9.61 m $yr^{-1}°C^{-1}$. This is similar to the differences in the melt rates for temperatures at the lower end of Table 4. These changes in the maximum melt rates are also more relevant to possible rates of ice thickness change near the ice shelf grounding line.

Nicholls (1997) has suggested that the response of the Filchner–Ronne Ice Shelf to ocean warming would be for it to thicken; that is, net melting from the ice shelf would decrease. In estimating this response Nicholls assumed that the seasonal variation of about 0.1°C, observed in oceanographic moorings under the Ronne Ice Shelf is analogous to the effects of climate warming. In calculating this estimate Nicholls assumed the Southern Weddell Sea circulation remains unchanged, particularly the domination of HSSW on the continental shelf and in the ocean cavity under the ice shelf. A constant ocean circulation ensures that the heat flux across the ice front is only able to vary because of temperature change. The results from the present study and that of Grosfeld and Gerdes (1998), show this is probably not a valid assumption, as both studies have found the internal circulation to be dependent on the temperature and salinity at the ice front. The results in this study also suggest that thickening of the ice shelf is unlikely to happen without cooling of the open ocean temperatures. The long-term applicability of Nicholls (1997) assumptions also need to be questioned. In the warming scenarios presented here the temperature increases in the south of the domain are about an order of magnitude more than the seasonal change observed by Nicholls. This would suggest that observed seasonal change may not be a reliable guide for estimating the effects of significant climate change under ice shelves.

Our results may have ramifications beyond the scope of this study. The changes in the basal component of the ice shelf mass balance indicate that the ice shelf mass budget will change significantly under expected climate change scenarios proposed for the next few hundred years. The present estimates of ice input to the Amery Ice Shelf are approximately 46 Gt yr^{-1}, and while the snow accumulation over the ice shelf would be expected to increase with global warming in such a coastal location, it is realistic to expect that such marked changes in the basal mass budget will lead to changes in ice shelf geometry and dynamics, particularly at the ice front and grounding lines. Any changes that might occur in grounding line positions, or ice shelf thickness could also impact upon the glaciers flowing into the ice shelf, potentially increasing flow in these glaciers due to a reduction in the restrictions from the ice shelf.

The results presented here show general agreement with results from studies of other ice shelves (Jenkins 1991; Hellmer and Jacobs 1995; Grosfeld and Gerdes 1998). The trend in all these studies was for an increase in melting with an increase in ocean temperature. This agreement between the different studies suggests the increased melting in response to warming found in this study may be indicative of the changes to be expected for other large Antarctic ice shelves in response to ocean warming around Antarctica.

Acknowledgments. The code for the numerical model was kindly provided by Jüergen Determann, Rüdiger Gerdes, and Klaus Grosfeld, Alfred Wegener Institute for Polar and Marine Research, Bremerhaven, Germany. We thank Nathan Bindoff, John Hunter, and the two anonymous reviewers for their comments. We thank Siobhan O'Farrell for providing the temperature anomaly data for Fig. 1.

APPENDIX

Ice–Ocean Boundary Conditions

The boundary conditions at the ice–ocean interface are derived from the three-equation formula described by Holland and Jenkins (1999). Here details of the equations as incorporated into the model used in this study are summarized. Full details of the arguments used in their derivation are given in Holland and Jenkins.

The ice shelf–ocean interface is assumed to be at the pressure-dependent freezing temperature, which is given by

$$T_b = -aS_b + b - cP_b, \tag{A1}$$

where T_b, S_b, and P_b are, respectively, the temperature, salinity, and pressure at the interface, and a, b, and c are, respectively, 0.0573°C psu^{-1}, 0.0939°C, and 7.53 $\times 10^{-8}$°C Pa^{-1}.

The heat flux balance at the ice–ocean interface can be described by the following equation:

$$Q^t_{\text{latent}} = Q^t_i - Q^t_w, \tag{A2}$$

where Q^t_{latent} is the latent heat released at the interface, Q^t_i is the conductive heat through the ice shelf, and Q^t_w is the diffusive heat flux from the upper-ocean layer. Following the three-equation formula of Holland and Jenkins these fluxes are defined as

$$Q^t_{\text{latent}} = -\rho_w mL, \tag{A3}$$

$$Q^t_i = -\rho_w C_{pi} w_i (T_s - T_b), \tag{A4}$$

$$Q^t_w = -\rho_w C_{pw} \gamma_t (T_b - T_w), \tag{A5}$$

where ρ_w is the density in the water layer (1028.0 kg m^{-3}), m is the melting (or freezing) rate of ice at the interface, L is the latent heat of fusion (3.34×10^5 J kg^{-1}), T_s is the temperature at the top ice shelf surface (−20°C), C_{pi} is the specific heat capacity of the ice (2009.0 J $kg^{-1}°C^{-1}$), C_{pw} is the specific heat capacity of the water (3974.0 J $kg^{-1}°C^{-1}$), and T_w is the temperature of the top ocean model layer. The vertical ve-

locity of the ice shelf, w_i, which is required to calculate the heat flux into the ice, is dependent on the state of melting or freezing:

$$\text{melting:} \quad m > 0 \quad w_i = m, \tag{A6}$$

$$\text{freezing:} \quad m < 0 \quad w_i = 0. \tag{A7}$$

The velocity-dependent mixing parameter, γ_t, for this study is calculated from the following equation (Jenkins 1991):

$$\gamma_t = \frac{u_*}{2.12 \ln(u_* h/\nu) + 12.5 \, \mathrm{Pr}^{2/3} - 9}, \tag{A8}$$

where h is the thickness of the top ocean model layer, ν is the viscosity of seawater (1.95×10^{-6} m^2 s^{-1}), and Pr (the molecular Prandtl number) is the dimensionless ratio of viscosity to thermal diffusivity (13.8). The friction velocity at the ice shelf, u_*, is calculated from the product of the speed of the top model layer and the square root of a dimensionless drag coefficient (1.5×10^{-3}).

The equations for salt conservation at the ice–ocean interface are similar to those for the heat exchange, except that the ice shelf is assumed to have a salinity of zero and not conduct salt. This gives a flux balance of

$$Q^s_{\text{brine}} = -Q^s_w, \tag{A9}$$

where Q^s_{brine} is the salt flux associated with brine rejection and Q^s_w is the diffusive salt flux in the ocean. These fluxes are defined as

$$Q^s_{\text{brine}} = -\rho_w m S_b, \tag{A10}$$

$$Q^s_w = -\rho_w \gamma_s (S_b - S_w), \tag{A11}$$

where S_w is the salinity of the water and γ_s is the velocity-dependent mixing parameter for salt. It is calculated in a similar way to γ_t, but with the Prandtl number replaced with the molecular Schmidt number (2432), which is the ratio of viscosity to salinity diffusivity.

REFERENCES

Budd, W. F., and X. Wu, 1998: Modelling long term global and Antarctic changes resulting from increased greenhouse gases. Coupled Climate Modelling, P. J. Meighen, Ed., BMRC Research Rep. 69, 71–74.

——, D. Jenssen, E. Mavrakis, and B. Coutts, 1994: Modelling the Antarctic ice-sheet changes through time. *Ann. Glaciol.,* **20,** 291–297.

Determann, J., and R. Gerdes, 1994: Melting and freezing beneath ice shelves: Implications from a three-dimensional ocean-circulation model. *Ann. Glaciol.,* **20,** 413–419.

El-Tahan, M., S. Venkatesh, and H. El-Tahan, 1987: Validation and quantitative assessment of the deterioration mechanisms of Arctic icebergs. *J. Offshore Mech. Arctic Eng.,* **109,** 102–108.

Gent, P. R., and J. C. McWilliams, 1990: Isopycnal mixing in ocean circulation models. *J. Phys. Oceanogr.,* **20,** 150–155.

Gerdes, R., J. Determann, and K. Grosfeld, 1999: Ocean circulation beneath Filchner–Ronne Ice Shelf from three-dimensional model results. *J. Geophys. Res.,* **104,** 15 827–15 842.

Grosfeld, K., and R. Gerdes, 1998: Circulation beneath the Filchner Ice Shelf and its sensitivity to changes in the oceanic environment: A case study. *Ann. Glaciol.,* **27,** 99–104.

——, ——, and J. Determann, 1997: Thermohaline circulation and interaction between ice shelf cavities and the adjacent open ocean. *J. Geophys. Res.,* **102,** 15 595–15 610.

Hamley, T. C., and W. F. Budd, 1986: Antarctic iceberg distribution and dissolution. *J. Glaciol.,* **32,** 242–251.

Hellmer, H. H., and D. J. Olbers, 1989: A two-dimensional model for the thermohaline circulation under an ice shelf. *Antarct. Sci.,* **1,** 325–336.

——, and ——, 1991: On the thermohaline circulation beneath the Filchner–Ronne Ice Shelves. *Antarct. Sci.,* **3,** 433–442.

——, and S. S. Jacobs, 1992: Ocean interactions with the base of Amery Ice Shelf, Antarctica. *J. Geophys. Res.,* **97,** 20 305–20 317.

——, and ——, 1995: Seasonal circulation under the eastern Ross Ice Shelf, Antarctica. *J. Geophys. Res.,* **100,** 10 873–10 885.

Hirst, A. C., 1999: The Southern Ocean response to global warming in the CSIRO coupled ocean–atmosphere model. *Environ. Modell. Software,* **14,** 227–241.

——, H. B. Gordon, and S. P. O'Farrell, 1996: Response of a coupled ocean–atmosphere model including eddy-induced advection to anthropogenic CO_2 increases. *Geophys. Res. Lett.,* **23,** 3361–3364.

Holland, D. M., and A. Jenkins, 1999: Modeling thermodynamic ice–ocean interactions at the base of an ice shelf. *J. Phys. Oceanogr.,* **29,** 1787–1800.

Huybrechts, P., and J. de Wolde, 1999: The dynamic response of the Greenland and Antarctic ice sheets to multiple-century climatic warming. *J. Climate,* **12,** 2169–2188.

Jacobs, S. S., H. H. Hellmer, C. S. M. Doake, A. Jenkins, and R. M. Frolich, 1992: Melting of ice shelves and the mass balance of Antarctica. *J. Glaciol.,* **38,** 375–387.

Jenkins, A., 1991: A one-dimensional model of ice shelf–ocean interaction. *J. Geophys. Res.,* **96,** 20 671–20 677.

——, and A. Bombosch, 1995: Modeling the effects of frazil ice crystals on the dynamics and thermodynamics of ice shelf water plumes. *J. Geophys. Res.,* **100,** 6967–6981.

Leggett, J., W. J. Pepper, and R. J. Swart, 1992: Emissions scenarios for the IPCC: An update. *Climate Change 1992: The Supplementary Report to the IPCC Scientific Assessment,* J. T. Houghton, B. A. Callander, and S. K. Varney, Eds., Cambridge University Press, 69–95.

MacAyeal, D. R., 1985: Evolution of tidally triggered meltwater plumes below ice shelves. *Oceanology of the Antarctic Continental Shelf,* S. S. Jacobs, Ed., Antarctic Research Series, Vol. 43, Amer. Geophys. Union, 133–143.

Manabe, S., and R. Stouffer, 1994: Multiple-century response of a coupled ocean–atmosphere model to an increase of atmospheric carbon dioxide. *J. Climate,* **7,** 5–23.

Nicholls, K. W., 1997: Predicted reduction in basal melt rates of an Antarctic ice shelf in a warmer climate. *Nature,* **388,** 460–462.

O'Farrell, S. P., J. L. McGregor, L. D. Rotstayn, W. F. Budd, C. Zweck, and R. Warner, 1997: Impact of transient increases in atmospheric CO_2 on the accumulation and mass balance of the Antarctic ice sheet. *Ann. Glaciol.,* **25,** 137–144.

Russell-Head, D. S., 1980: The melting of free-drifting icebergs. *Ann. Glaciol.,* **1,** 119–122.

Stevens, D. P., 1990: On open boundary conditions for three dimensional primitive equation ocean circulation models. *Geophys. Astrophys. Fluid Dyn.,* **51,** 103–133.

Warner, R. C., and W. F. Budd, 1998: Modelling the long-term response of the Antarctic ice sheet to global warming. *Ann. Glaciol.,* **28,** 161–168.

Williams, M. J. M., 1999: A numerical study of ocean circulation and ice–ocean interaction, beneath the Amery Ice Shelf, Antarctica. Ph.D. thesis, University of Tasmania, Hobart, Australia, 261 pp.

——, A. Jenkins, and J. Determann, 1998a: Physical controls on ocean circulation beneath ice shelves revealed by numerical

models. *Ocean, Ice, and Atmosphere: Interactions at the Antarctic Continental Margin*, S. S. Jacobs and R. F. Weiss, Eds., Antarctic Research Series, Vol. 75, Amer. Geophys. Union, 285–299.

——, R. C. Warner, and W. F. Budd, 1998b: The effects of ocean warming on melting and ocean circulation under the Amery Ice Shelf, East Antarctica. *Ann. Glaciol.,* **28,** 75–80.

——, K. Grosfeld, R. C. Warner, R. Gerdes, and J. Determann, 2001: Ocean circulation and ice–ocean interaction beneath the Amery Ice Shelf, Antarctica. *J. Geophys. Res.*, **106,** 22 383–22 399.

Wong, A. P. S., N. L. Bindoff, and A. Forbes, 1998: Ocean–ice shelf interaction and possible bottom water formation in Prydz Bay, Antarctica. *Ocean, Ice, and Atmosphere: Interactions at the Antarctic Continental Margin*, S. S. Jacobs and R. F. Weiss, Eds., Antarctic Research Series, Vol. 75, Amer. Geophys. Union, 173–187.